

# CRITICAL BEHAVIOR OF THE SCHWINGER MODEL WITH WILSON FERMIONS

V. Azcoiti<sup>a</sup>, G. Di Carlo<sup>b</sup>, A. Galante<sup>c,b</sup>, A.F. Grillo<sup>d</sup>, and V. Laliena<sup>a</sup>

<sup>a</sup> *Departamento de Física Teórica, Facultad de Ciencias, Universidad de Zaragoza, 50009 Zaragoza (Spain).*

<sup>b</sup> *Istituto Nazionale di Fisica Nucleare, Laboratori Nazionali di Frascati, P.O.B. 13 - Frascati 00044 (Italy).*

<sup>c</sup> *Dipartimento di Fisica dell'Università dell'Aquila, L'Aquila 67100 (Italy)*

<sup>d</sup> *Istituto Nazionale di Fisica Nucleare, Laboratori Nazionali del Gran Sasso, Assergi (L'Aquila) 67010 (Italy).*

## ABSTRACT

We present a detailed analysis, in the framework of the MFA approach, of the critical behaviour of the lattice Schwinger model with Wilson fermions on lattices up to  $24^2$ , through the study of the Lee-Yang zeros and the specific heat. We find compelling evidence for a critical line ending at  $\kappa = 0.25$  at large  $\beta$ . Finite size scaling analysis on lattices  $8^2, 12^2, 16^2, 20^2$  and  $24^2$  indicates a continuous transition. The hyperscaling relation is verified in the explored  $\beta$  region.

## 1. Introduction

Although apparently far from physical reality, the Schwinger model, i.e., the theory describing the interaction between photons and electrons in  $1 + 1$  dimensions, has been a favourite framework for theoretical and numerical exercises for at least two reasons.

First, the massless Schwinger model can be analytically solved in the continuum and this is the reason why it has always been used as a laboratory for the development of numerical algorithms for dynamical fermions.

Second, and due to the special low dimensionality dynamics, this model shares many physical properties with four dimensional  $QCD$ , the gauge theory describing the strong interaction of hadrons. In fact the charge is confined in the Schwinger model and long range forces are absent in it. Of course the Schwinger model has also some characteristic features which are not common to  $QCD$  like the property of superrenormalizability or ultraconfinement (it effectively describes free bosons) and the absence of the Goldstone boson. However we expect a phase diagram in the lattice regularized Schwinger model qualitatively similar to that of lattice  $QCD$ , in particular since, as can be derived from dimensional arguments, the continuum limit is reached at infinite gauge coupling. This is one of the motivations for this paper.

The Schwinger model on the lattice, using the Kogut-Susskind regularization for the fermion fields, has been the subject of extensive analysis. The phase structure of the model in the gauge coupling  $\beta$  and fermion mass  $m$  plane is well known and the continuum value for the chiral condensate has been reproduced within three decimal places [1], the best numerical result to our knowledge, using the *MFA* approach [2]. In the Wilson regularization for fermion fields however, the situation is not so clear. In this scheme, chiral symmetry is explicitly broken even for vanishing bare fermion mass and this is the unavoidable price to pay to overcome the species doubling problem. Therefore no order parameter can be used for analyzing the phase diagram, which besides the larger number of degrees of freedom if compared with the Kogut-Susskind regularization, makes the analysis far from trivial.

Furthermore almost all the standard algorithms to simulate numerically dynamical fermions, like hybrid Monte Carlo, which are based on the inclusion of the fermion determinant in the integration measure, need to duplicate the number of fermion species in order to avoid negative values for the determinant of the Dirac operator, which makes impossible to investigate the phase structure of the one flavour Schwinger model. This is the reason why until very recent time, when an analysis of the phase diagram of the Schwinger model in the Wilson regularization using non standard methods

was performed [3], very little was known about it.

In this article we will report the results of a numerical simulation of the one flavour Schwinger model in the Wilson regularization, by means of *MFA* simulations. The structure of the Lee-Yang zeroes in the complex hopping parameter  $\kappa$  plane strongly suggests the existence of a critical line: in our simulations the critical  $\kappa$  is 0.27 at  $\beta = 2$ , ending at  $\kappa = 0.25$ ,  $\beta \rightarrow \infty$ , the critical point where the continuum limit is recovered. We also describe results concerning the specific heat showing a sharp peak along a line  $\kappa_c = f(\beta_c)$  in the  $\kappa, \beta$  plane, in good numerical agreement with predictions from the Lee-Yang zeros analysis. The results of the finite size scaling analysis for the Lee-Yang zeros and chiral susceptibility allow the determination of the critical exponents, and the fulfillment of the hyperscaling relation gives a definite confirmation that we are dealing with a real second order phase transition line.

## 2. Theoretical Grounds

The lattice action for the massive Schwinger model with Wilson fermions is given by

$$S(\beta, \kappa) = S_F(\kappa) + \beta S_G \quad (1)$$

where  $S_F(\kappa)$  contains the kinetic and mass terms for the fermion field as well as the fermion-gauge interaction term, and we have chosen for the pure gauge action  $S_G$  the standard noncompact regularization for the abelian model. The fermionic action  $S_F(\kappa)$  reads

$$\begin{aligned} S_F(\kappa) = \kappa \sum_{\mu, x} [ & \bar{\psi}(x + \mu)(1 + \gamma_\mu)U_\mu^\dagger(x)\psi(x) \\ & + \bar{\psi}(x)(1 - \gamma_\mu)U_\mu(x)\psi(x + \mu)] - \sum_x \bar{\psi}(x)\psi(x) \end{aligned} \quad (2)$$

Equation (2) defines the Dirac matrix operator  $\Delta$  which can be written as

$$\Delta = -I + \kappa M \quad (3)$$

where  $I$  is the unit matrix and  $M$  a matrix of dimension equal to the lattice volume times the number of Dirac components.

The use of the *MFA* approach in the numerical simulations of the system described by action (1) has at least two very important advantages when

compared with other standard approaches. First, since *MFA* is based on the computation of the fermion effective action defined as the logarithm of the mean value of the fermion determinant at fixed pure gauge energy and this mean value is positive definite at least in the physically interesting region, we have no problems to simulate the one flavour model. Secondly, since the  $\kappa$  dependence factorizes in the non trivial part of the fermionic operator (3), we do not need to repeat the numerical simulations when changing the value of the hopping parameter  $\kappa$ , which is mandatory for exploring the zeros of the partition function in the complex  $\kappa$  plane. Let us notice also that, while *MFA* has been extensively used and checked in lattice gauge theories with Kogut-Susskind fermions, this is the first time it is applied to a lattice model with Wilson fermions.

The technical details of *MFA* can be found by the interested reader in refs. [2]. As stated before, all the applications of *MFA* to lattice gauge theories in these references were done using staggered fermions. The main difference between staggered and Wilson fermions comes from the different structure that the Dirac operator has in each formulation. In the Wilson case, where the fermion matrix has the structure given by equation (3), the *MFA* approach works as follows: first we generate well decorrelated gauge field configurations at fixed noncompact gauge energy

$$E = \frac{1}{V} \sum_{x, \mu < \nu} (A_\mu(x) + A_\nu(x + \mu) - A_\mu(x + \nu) - A_\nu(x)) \quad (4)$$

and then we diagonalize the  $M$  matrix for each generated configuration. Due to the non hermiticity of the matrix we can not use the standard Lanczos algorithm; the eigenvalues are found using a standard library diagonalization routine. From the eigenvalues of the  $M$  matrix we can reconstruct the determinant of the Dirac operator  $\Delta$  at any value of the hopping parameter  $\kappa$  in a trivial way. The partition function associated to the action (1) can be written then as

$$Z(\beta, \kappa) = \sum_n C_n(\beta) \kappa^n = \int dE n(E) e^{-\beta V E} \sum_n C_n(E) \kappa^n \quad (5)$$

where  $n(E)$  is the density of states at fixed pure gauge energy and  $C_n(E)$  in (5) stands for the mean value of the  $n$ th coefficient of the polynomial describing the fermionic determinant, the average being computed over gauge field configurations at fixed pure gauge energy, i.e.,

$$C_n(E) = \int [dA_\mu] C_n(A_\mu(x)) \delta\left(\sum_{x,\mu<\nu} (A_\mu(x) + A_\nu(x+\mu) - A_\mu(x+\nu) - A_\nu(x)) - VE\right) \quad (6)$$

Since the density of states at fixed pure gauge energy

$$n(E) = \int [dA_\mu] \delta\left(\sum_{x,\mu<\nu} (A_\mu(x) + A_\nu(x+\mu) - A_\mu(x+\nu) - A_\nu(x)) - VE\right) \quad (7)$$

can be analytically computed in the noncompact model, we can reconstruct the partition function (5) from the knowledge of the coefficients  $C_n(E)$  through interpolation and one-dimensional integration. Had we used the more standard compact Wilson formulation for the gauge fields, the standard procedure would be very similar with the only difference that in such a case, the density of states, in general, would have to be computed numerically.

If on the other hand we are interested in the computation of vacuum expectation values of physical operators like the chiral condensate, the standard procedure is the one described in [2]. We will not repeat here the details of this procedure but only will remember that it is based on the computation of the fermion effective action as a function of the gauge energy and the computation of the mean value of the operator times the fermion determinant over gauge field configurations of fixed pure gauge energy.

### 3. The Lee-Yang zeros in the complex $\kappa$ plane.

The first step to the determination of the position of the Lee-Yang zeros in the complex  $\kappa$  plane is the computation of the coefficients  $C_n(E)$  of the averaged determinant of the Dirac operator. For the calculation of  $C_n(E)$  we proceed as follows: first we chose a set of values of energy, in the range selected to cover the support of the weight function in (5) for the values of  $\beta$  we are interested in. Then for every value of  $E$  in the set we generate gauge field configurations using a microcanonical code; the generation of gauge fields at fixed energy is not the costly part of the whole procedure, so we can well decorrelate the configurations used for measuring the fermionic operator. Then, as stated before, we compute exactly the eigenvalues of the  $M$  matrix from which we reconstruct by a recursion formula the coefficients of the fermionic determinant.

At the end we have the coefficients  $C_n(E)$  evaluated at discrete energy values: a polynomial interpolation allows the reconstruction at arbitrary

values of the energy  $E$ , in order to perform the numerical integration in (5) and obtain the coefficients  $C_n(\beta)$  that can be regarded as the final product of this part of the numerical procedure for the determination of the Lee Yang zeros. These coefficients are then used for the determination of the roots of the polynomial  $Z(\beta, \kappa)$ .

The main features of  $Z(\beta, \kappa)$  are the following: in a volume  $V$ , the partition function is a polynomial of order  $N = 2V$  in  $\kappa$  and the typical range of the coefficients is of order  $e^V$ . Thus, the main numerical problem is the efficiency of standard root finders in the determination of the zeros. Here we have used a method [4] developed in order to analyse the partition function zeros in the four dimensional compact  $U(1)$  model. This algorithm is based on well known properties of analytic functions on the complex plane which, in particular, allows the determination of the number of zeros for a given function inside a region of the complex plane, provided the function has no singularities inside this region.

In Figure 1 we plot the location of all the zeros (in the complex  $\kappa$  plane) in a  $16^2$  lattice at  $\beta = 7$ . Figures 2 a,b contain the zeros closest to the real axis in all the lattices used at  $\beta = 7, 10$

To estimate the statistical errors on the position of the Lee-Yang zeros we followed the procedure described in [4]: a standard jack-knife method is used to produce  $n$  averaged partition functions and  $n$  estimates of the location of a given zero. The largest error on the distance of critical zeros (those with smallest imaginary part) with respect to the free fermion critical point (0.25,0.0) is of order 2%. In all the cases reported in these figures, we can see how the nearest zero to the real axis approaches it with increasing lattice size, thus suggesting the existence of a phase transition line in the  $\beta - \kappa$  plane.

In Figure 3 we show the phase diagram in the  $\beta - \kappa$  plane obtained from  $8^2$ ,  $16^2$  and  $24^2$  lattices. The real part of the location of the zero lying nearest to the real axis gives an estimate of the value of the critical  $\kappa$ . Note that the critical line moves upward with increasing volume.

A detailed analysis of the scaling behavior for the Lee-Yang zeros and  $\kappa_c$  with the lattice size will be presented in section 5.

At smaller values of  $\beta$  our procedure has some problems: the signature is the appearance of unphysical real zeros at finite volume, so that the estimation of the critical point becomes unsafe. This behaviour is related to the large fluctuations in the averaging procedure for the coefficients, already pointed out in [3]. Nevertheless, if we take the zeros with smaller, but not zero, imaginary part as the critical zeros we can continue the critical line

down to  $\beta = 0$ , ending at  $k_c = 0.36$  for a  $8^2$  lattice and  $k_c = 0.35$  for a  $16^2$  lattice. Note that in [3] an exact result for the partition function at  $\beta = 0$  for a  $8^2$  lattice is reported, giving a critical point at  $k_c = 0.377$ .

#### 4. The specific heat.

Chiral symmetry is always explicitly broken and there is no order parameter in this realization of the model, so  $\kappa$  cannot be identified with an external field. We take it instead as a temperature, defining the the associated specific heat as usual:

$$C_\kappa = \frac{\partial^2 \mathcal{F}}{\partial \kappa^2}$$

where  $\mathcal{F}$  is the free energy density.

The specific heat is related to the chiral susceptibility  $\chi$ , defined as

$$\chi = -2\kappa^2 \frac{d}{d\kappa} \langle \bar{\psi}(x)\psi(x) \rangle \quad (8)$$

differing only through a regular function of  $\kappa$  which does not influences the critical behavior. The susceptibility, which is what we have measured, diverges at the transition in the thermodynamical limit, the divergence becoming a sharp peak on finite lattices.

The study of the position of the maximum at different lattice sizes gives a way to search for the phase transition line which is numerically independent from that presented in the previous section. We remind that, as the model is not chirally invariant, the analogy with a magnetic system fails.

Figures 4a,b contain the results for the susceptibility (8) at two typical values of the gauge coupling  $\beta$  against  $\kappa$  in  $8^2, 12^2, 16^2, 20^2$  and  $24^2$  lattices. As expected for a real phase transition, the susceptibility shows a well defined maximum at some critical value  $\kappa_c$ , the height of these peaks increasing with the lattice size and eventually diverging in the infinite volume limit. If we define the critical  $\kappa_c$  at each  $\beta$  as the value at which the susceptibility  $\chi$  takes its maximum value, we get for the lattices analyzed the phase diagram reported in Figure 5, in very good agreement, in the largest lattices, with the one obtained from the analysis of the Lee-Yang zeros.

#### 5. Finite size scaling analysis.

We will now present a detailed analysis of the scaling behavior for the

Lee-Yang zeros and specific heat, mainly based on simulations on  $16^2, 20^2$  and  $24^2$  lattices.

In the analysis of the phase diagram from the location of the Lee-Yang zeros of Figure 3, the real part of the zero lying next to the real axis defines the critical  $\kappa$  at each lattice size. In order to have a real phase transition, the imaginary part of the critical zero should vanish in the infinite volume limit. This has been explicitly checked by assuming that the imaginary part of the critical zero  $z_c(L)$  as a function of lattice size is described by the function

$$\text{Im } z_c(L) = a_0 + a_1 L^{-\frac{1}{\nu}}. \quad (9)$$

In all the  $\beta$  region explored, the value of  $a_0$  is compatible with zero. The scaling analysis at this point is made using the relations [5]

$$\begin{aligned} \kappa_c(L) - \kappa_c(\infty) &\sim L^{-\frac{1}{\nu}} \\ \text{Im } z_c(L) &\sim L^{-\frac{1}{\nu}}. \end{aligned} \quad (10)$$

for the real and imaginary parts of the critical zero.

In Figure 6 we show the typical scaling behavior as a function of the volume for the imaginary part of the critical zero, at  $\beta = 10$ . Similar results have been obtained at different  $\beta$ . From the slopes of the lines fitting the data from  $16^2, 20^2, 24^2$  we determine the scaling exponent  $\nu$  as a function of  $\beta$ . This is shown in Figure 7. The value of the critical index clearly indicates that the transition is continuous at any value of  $\beta$ . We note, moreover, that our results are compatible with  $\nu = \frac{2}{3}$ , at any  $\beta$ .

Concerning the susceptibility  $\chi$ , the critical  $\kappa$  reported in Figure 5 was defined, as stated before, as the value of  $\kappa$  at which the susceptibility takes its maximum value. Both the height  $H(L)$  of the peak as well as its position  $\kappa_c(L)$  depend on the lattice size  $L$ . Standard finite size scaling theory tell us that these quantities scale with the lattice size as [6]

$$H(L) \sim L^{\frac{\alpha}{\nu}} \quad (11)$$

where  $\alpha$  in (11) is the specific heat exponent.

In Figure 7 we present also the scaling index of  $H$  as a function of  $\beta$ . Its value is again consistent with a continuous phase transition. The value obtained implies  $\alpha \sim \nu$ .

Since in the critical region the singular part of the free energy behaves as:



$$\mathcal{F}_{sing} \sim (\kappa - \kappa_c)^{2-\alpha} \quad (12)$$

and given that the only relevant length in this region should be the correlation length, we get

$$\mathcal{F}_{sing} \sim \xi^{-d} \sim (\kappa - \kappa_c)^{d\nu} \quad (13)$$

from which the standard hyperscaling relation between the correlation length and specific heat exponents follows

$$d\nu = 2 - \alpha \quad (14)$$

Our data for the critical exponents satisfy relation (14) within the errors, in the whole  $5 < \beta < 12.5$  region; the typical deviation from (14) is of the order of 0.07.

We can conclude from the finite size scaling analysis of the Lee-Yang zeros and chiral susceptibility that the lattice Schwinger model with Wilson fermions has a real continuous phase transition ending at  $\beta_c = \infty, \kappa_c = 0.25$ . We are able to derive the critical exponents of the model and we find perfect agreement with the hyperscaling relation.

In Figure 8 we show the scaling behavior of the real part of the critical zero at  $\beta = 10$ . The infinite volume value of  $\kappa_c$  can be inferred using the Finite Size Scaling in (10). In principle this analysis, carried out for several values of  $\beta$ , could give an estimate of the infinite volume critical  $\kappa$  as a function of the gauge coupling constant. However it seems very difficult to get reliable values for  $\kappa_c(\infty)$  from the relation (10) for the real part of the critical zeros [7] since this is not a universal relation.

## 6. Discussion.

In the previous sections we have shown that the Schwinger model regularized on a lattice and with Wilson fermions has a continuous phase transition in the  $(\beta, \kappa)$  plane, where the correlation length diverges. The finite size scaling analysis shows a correlation length exponent  $\nu$  taking a value around  $2/3$  along this transition line, a result which appears very reliable since, as previously shown, the hyperscaling relation (14) is always verified. This value of  $\nu$  is in contrast with the value  $\nu = 1$  obtained at the end point  $\beta = \infty$  of the transition line as well as with the value, again  $\nu = 1$ , at  $\beta = 0$  suggested by the analysis reported in [7],[8]. We would like to notice that violations to Universality in fermionic systems, probably due to the long range forces

induced by the fermion fields, have been previously observed in the Gauged Nambu-Jona Lasinio model [9], [10] as well as in a fermion-gauge-scalar model [11].

Let us finally comment on the physical meaning of the continuous phase transition line. In  $QCD_4$  this transition line, whose existence and location are not as clear as here, is assumed to be the line along which the pion is massless. In two-dimensional models, as well known, Goldstone bosons are absent. Moreover, the correlation length which diverges in our case is that associated to the scalar particle, not the pseudoscalar one. Nevertheless, it is our prejudice that this is the line along which the fermion remains massless even if, due to the pathologies of two-dimensional models, massless scalars or pseudo-scalars are absent.

## **7. Acknowledgements.**

It is a pleasure to thank H. Gausterer and C.B. Lang for very interesting discussions and interchange of information.

This work has been partly supported through a CICYT (Spain) - INFN (Italy) collaboration.

## References

- [1] V. Azcoiti, G. Di Carlo, A. Galante, A.F. Grillo and V. Laliena, Phys. Rev. **D50** (1994) 6994.
- [2] V. Azcoiti, G. Di Carlo and A.F. Grillo, Phys. Rev. Lett. **65** (1990) 2239; V. Azcoiti, A. Cruz, G. Di Carlo, A.F. Grillo and A. Vladikas, Phys. Rev. **D43** (1991) 3487; V. Azcoiti, G. Di Carlo, L.A. Fernandez, A. Galante, A.F. Grillo, V. Laliena, X.Q. Luo, C.E. Piedrafita and A. Vladikas, Phys. Rev. **D48** (1993) 402. V. Azcoiti, G. Di Carlo, A. Galante, A.F. Grillo and V. Laliena, Phys. Rev. **D50** (1994) 6994.
- [3] H. Gausterer and C.B. Lang, Phys. Lett. **B341** (1994) 46.
- [4] V. Azcoiti, I.M. Barbour, R. Burioni, G. Di Carlo, A.F. Grillo and G. Salina, Phys. Rev. **D51** (1995) 5199.
- [5] C. Itzykson, R.B. Pearson and J.B. Zuber, Nucl. Phys. **B220** (1983) 415.
- [6] M.E. Fisher, in: Critical Phenomena, Proc. 51st Enrico Fermi Summer School, Varenna, ed. M.S. Green (Academic Press, New York, 1972); M.N.Barber, in: Phase Transitions and Critical Phenomena, Vol. 8, eds C. Domb and J.L. Lebowitz (Academic Press, London, 1983)
- [7] H. Gausterer and C.B. Lang, "Strong coupling lattice Schwinger model on large sphere-like lattices", **UNIGRAZ-UTP-27-06-95** (1995).
- [8] F. Karsch, E. Meggiolaro and L. Turko, Phys. Rev. **D51** (1995) 6417.
- [9] A. Kocic, S. Hands, J.B. Kogut and E. Dagotto, Nucl. Phys. **B347** (1990) 217.
- [10] V. Azcoiti, G. Di Carlo, A. Galante, A.F. Grillo, V. Laliena and C.E. Piedrafita, Phys. Lett. **B355** (1995) 270.
- [11] W. Franzki, C. Frick, J. Jersak and X.Q. Luo, **HLRZ 23/95** (1995).

## Figure captions

**Figure 1.** Position of all the zeros at  $\beta = 7.0$ ,  $16^2$  lattice.

**Figure 2.** Zeros closest to real axis,  $\beta = 7, 8^2, 12^2, 16^2, 20^2, 24^2, \beta = 10$  (b).

**Figure 3.**  $\beta - \kappa$  phase diagram from Lee-Yang zeros.

**Figure 4.** Chiral susceptibility versus  $\kappa$  at  $\beta = 6.9$  (a) and  $\beta = 9.9$  (b); the error shown is the typical one.

**Figure 5.**  $\beta - \kappa$  phase diagram from chiral susceptibility (upper curves),  $8^2, 16^2, 24^2$  lattices, the lines are the data of Figure 3.

**Figure 6.** Imaginary part of the critical zero versus lattice size  $L$ ,  $\beta = 10.0$ .

**Figure 7.**  $\nu$ ,  $\frac{\nu}{\alpha}$  versus  $\beta$ ,  $16^2, 20^2, 24^2$  lattices.

**Figure 8.** Real part of the critical zero versus  $L$ ,  $\beta = 10.0$ ; the line is the best fit using (10).

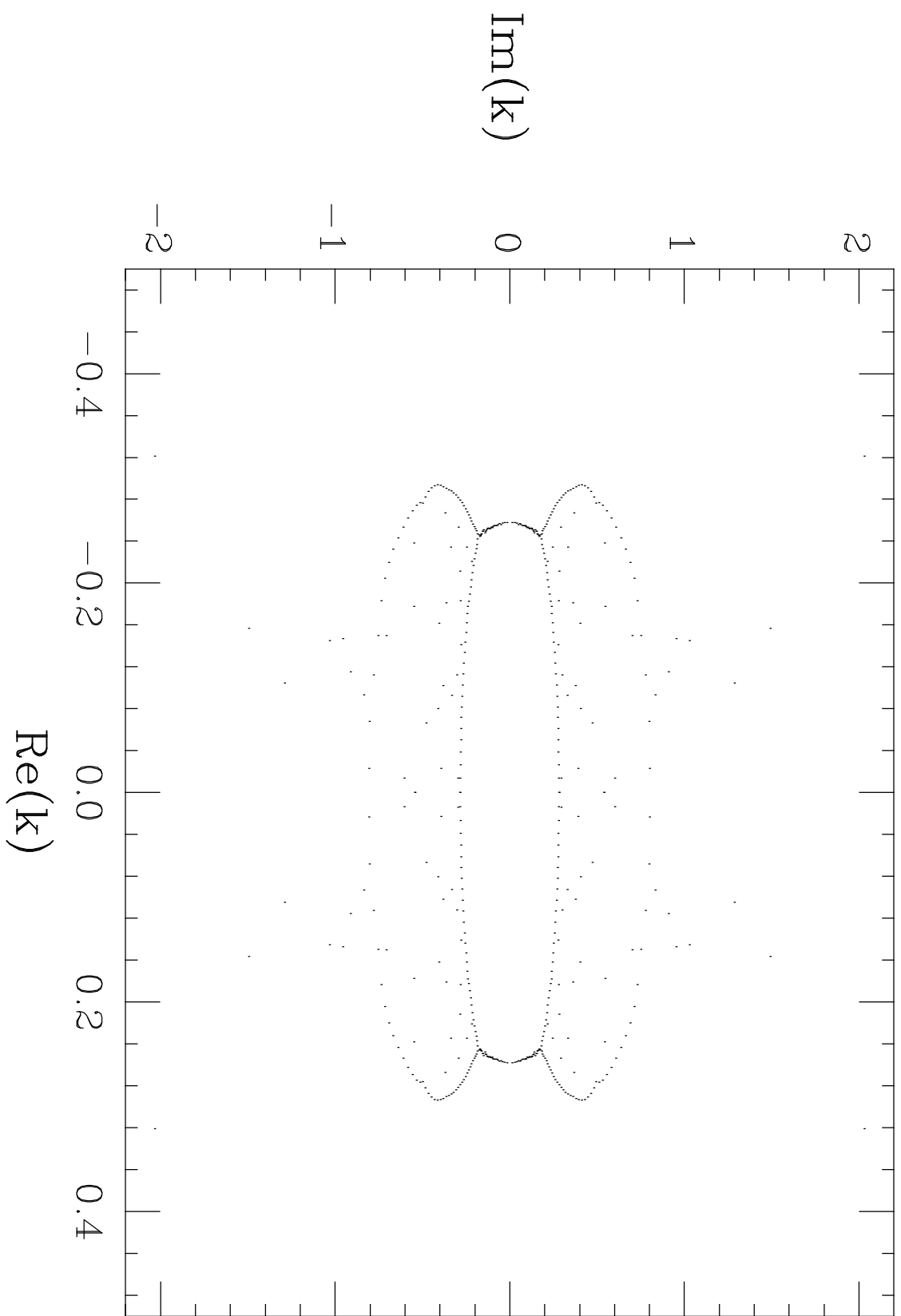


Fig. 1

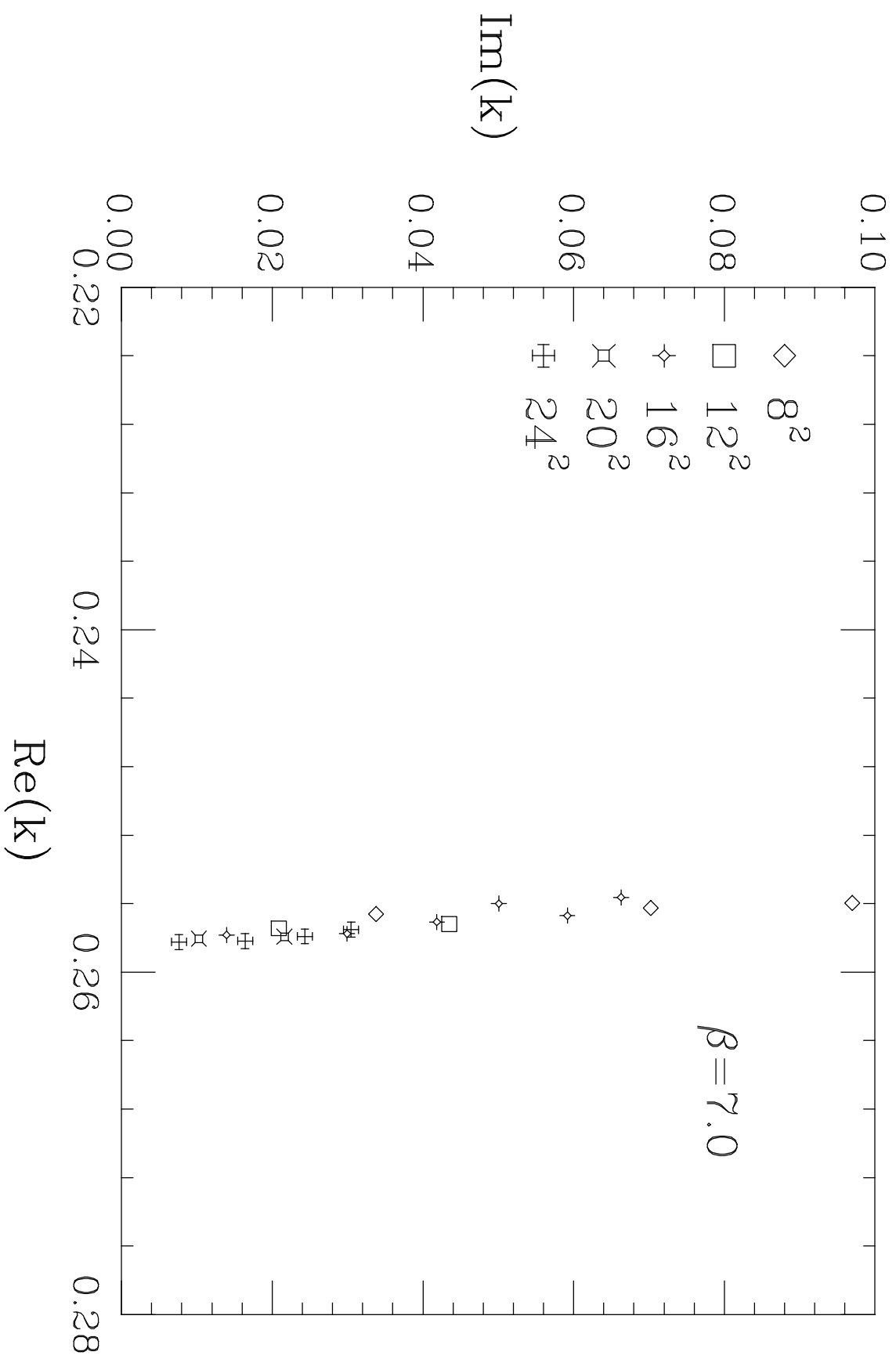


Fig. 2-a

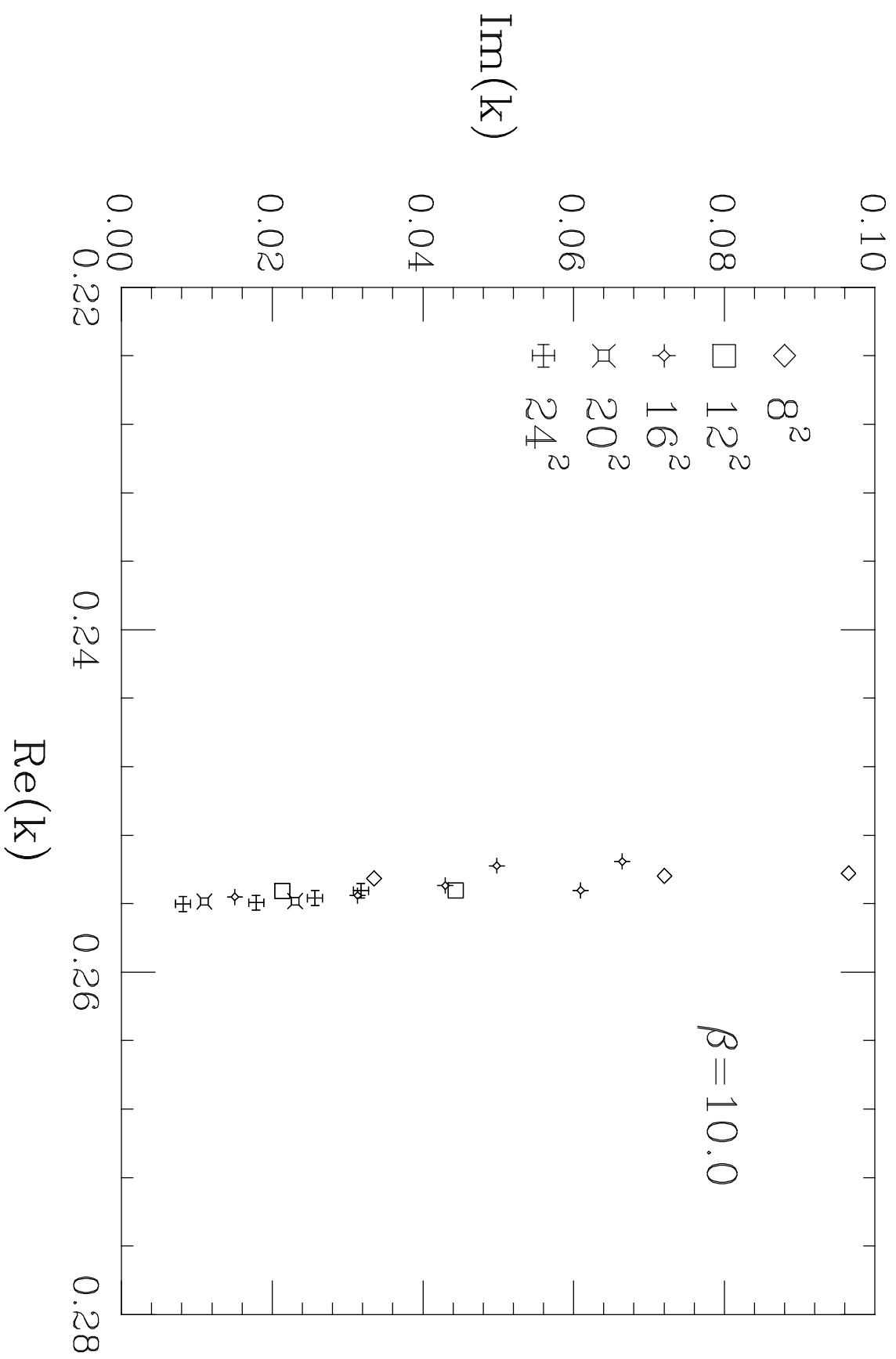


Fig. 2-b

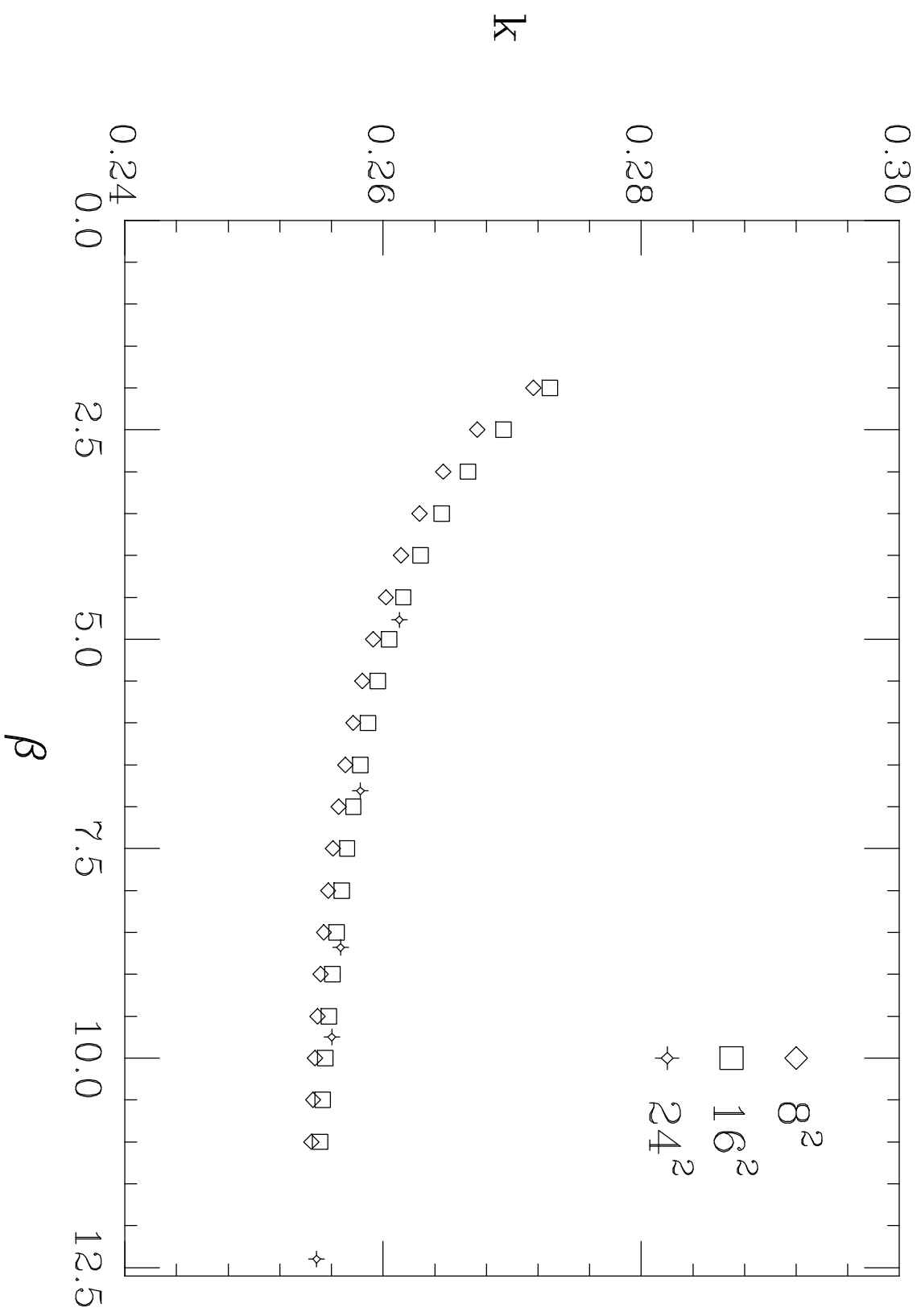


Fig. 3



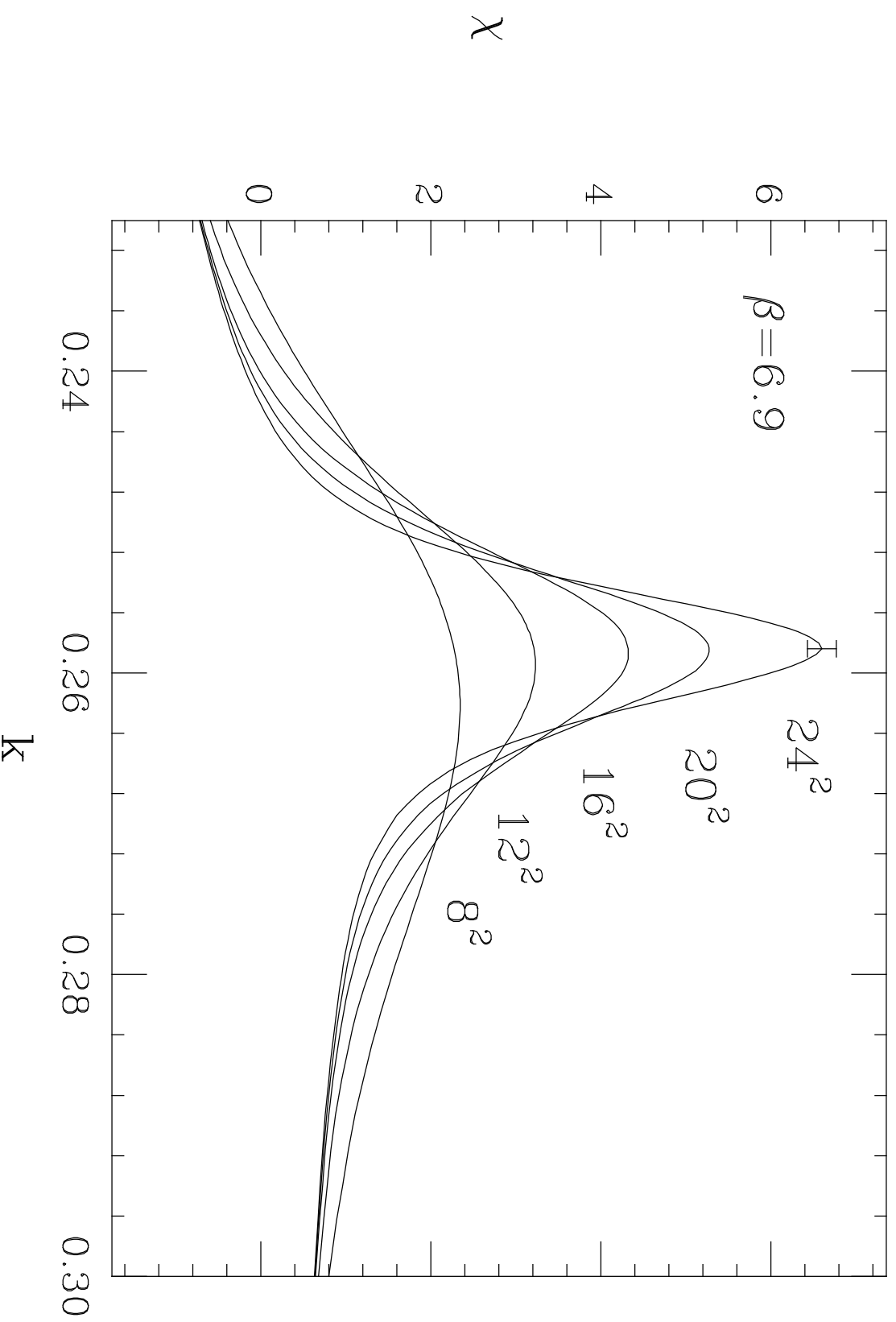


Fig. 4-a

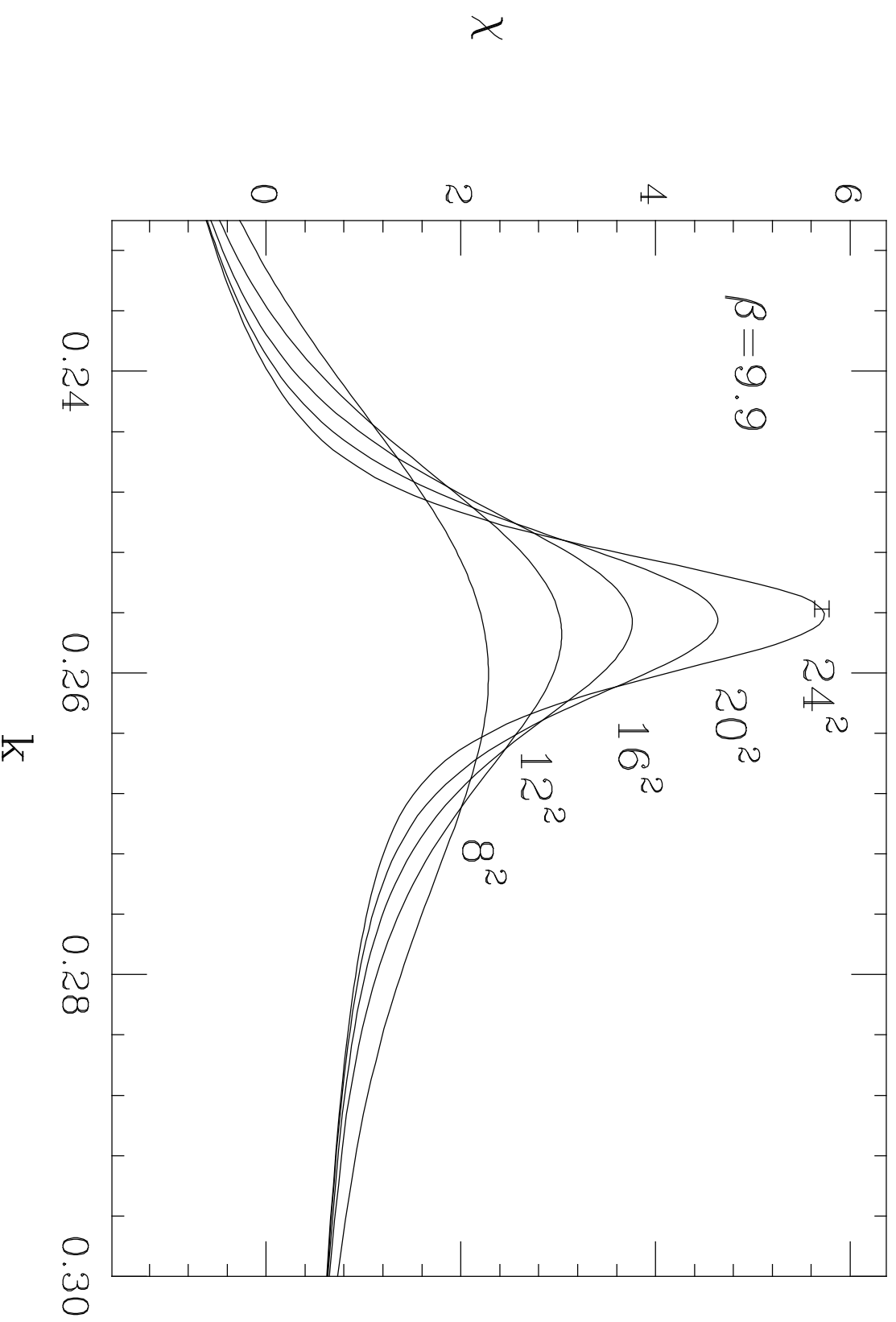


Fig. 4-b

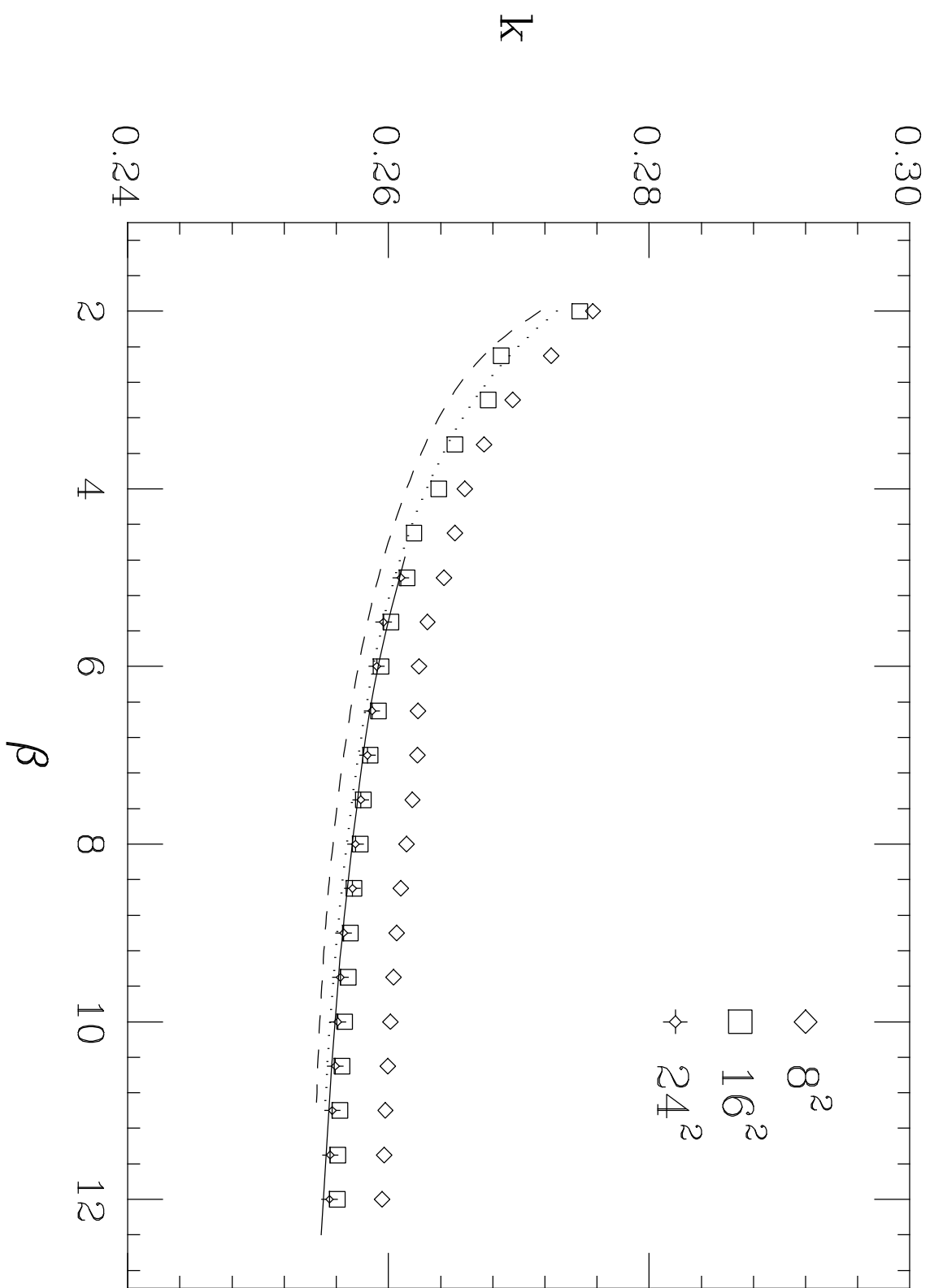


Fig. 5

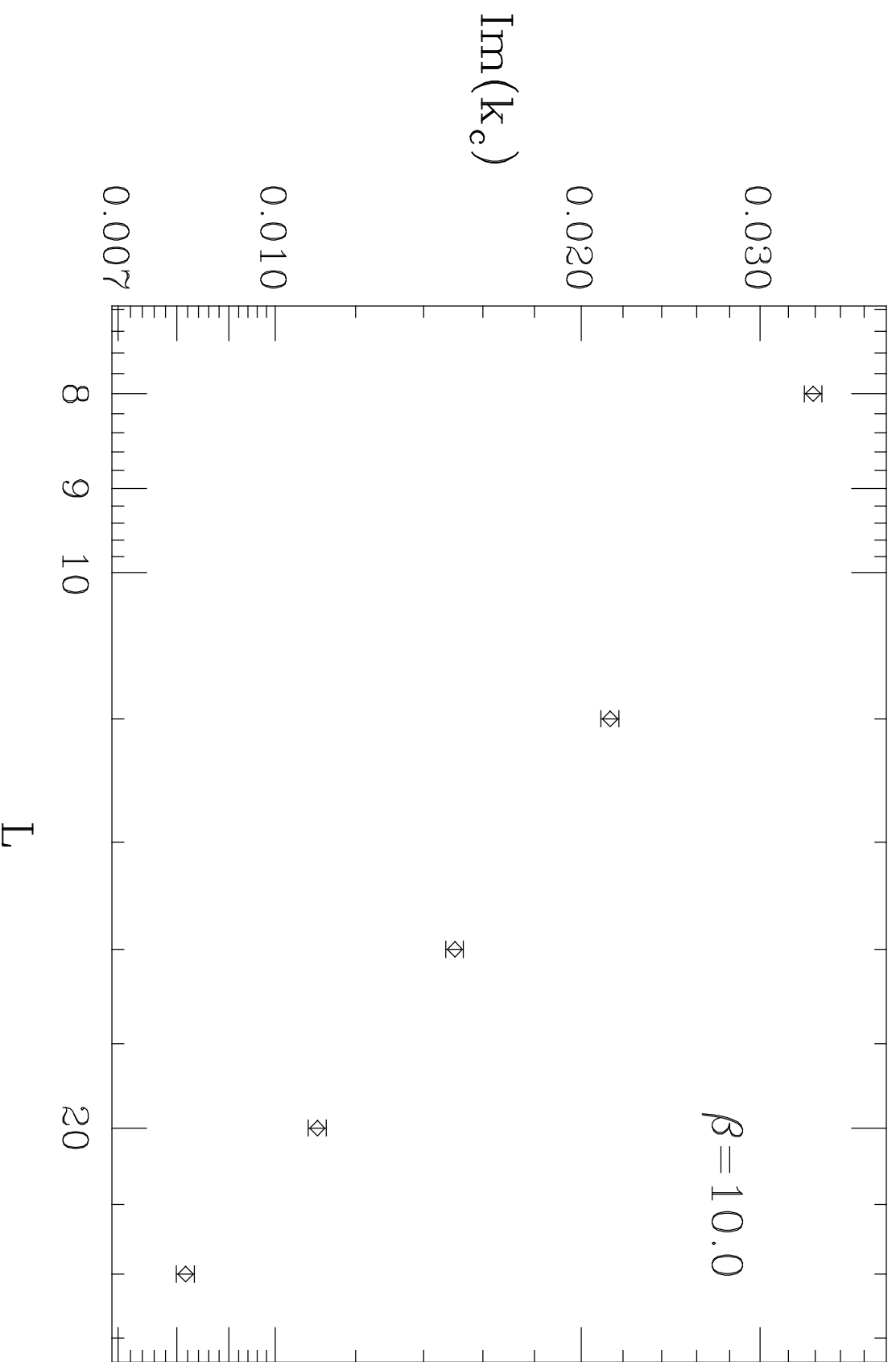


Fig. 6

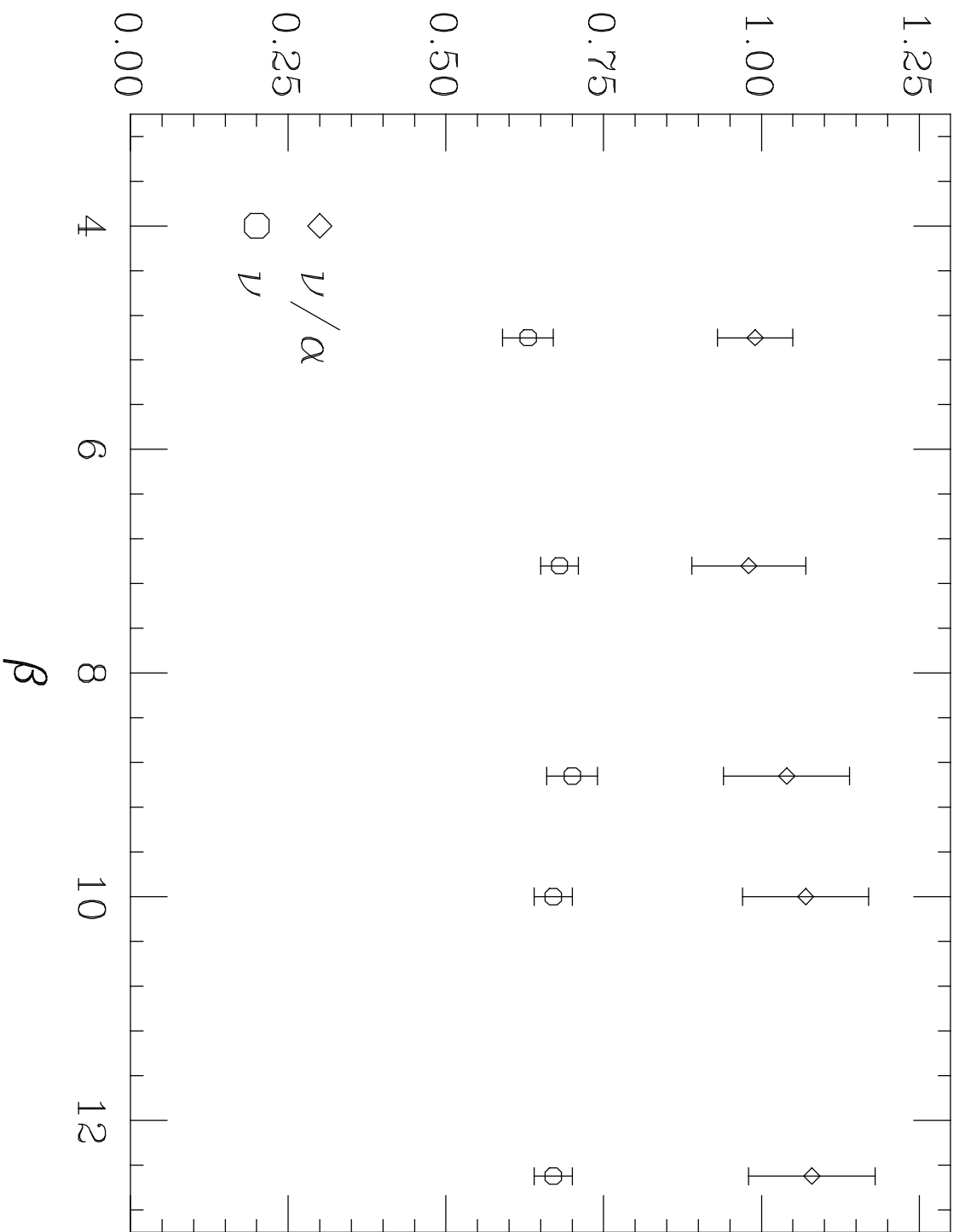


Fig. 7

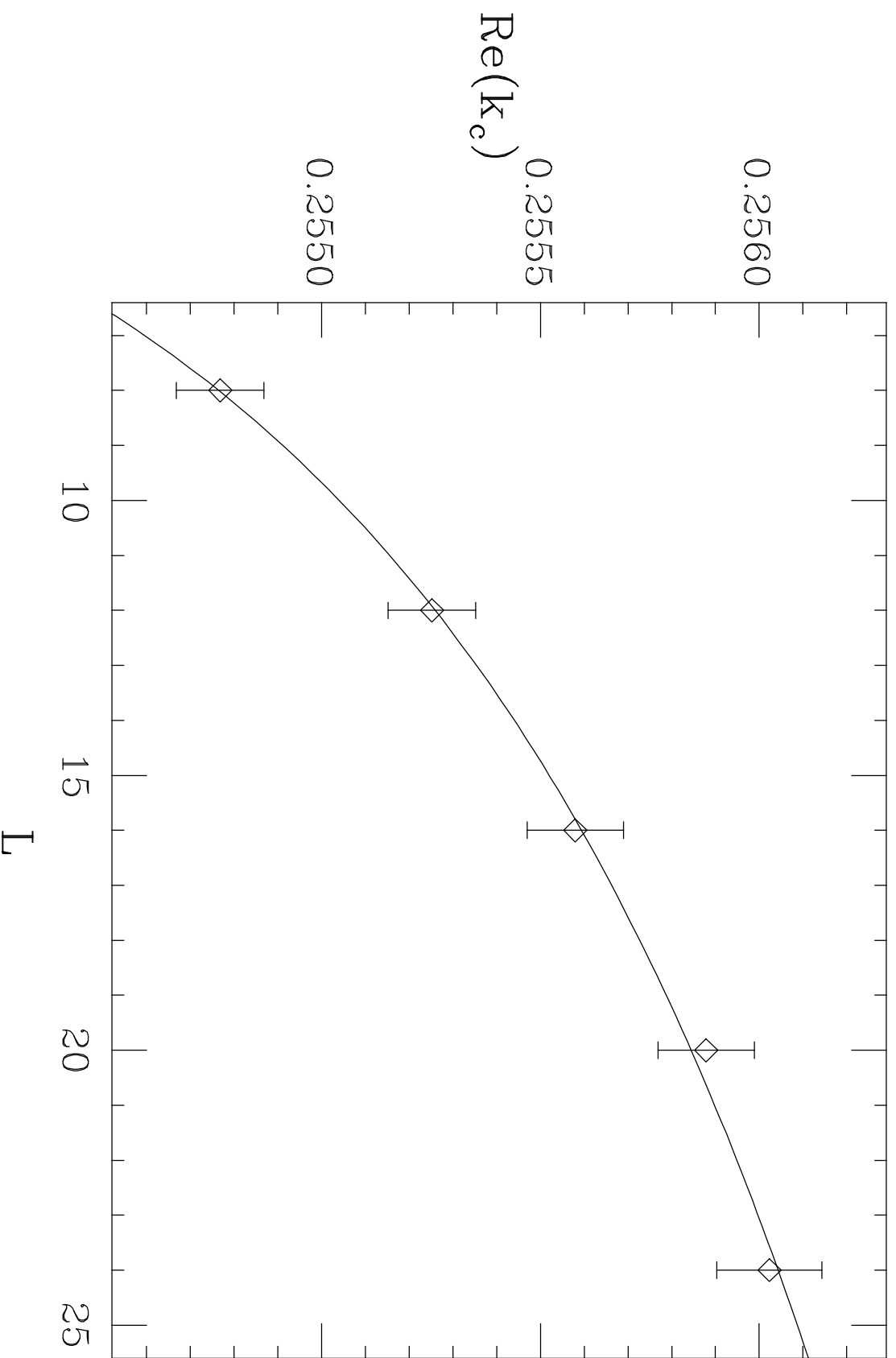


Fig. 8